NASA Technical Memorandum 102045
SWL89-2

A Segmented Mirror Antenna for Radiometers

S.W. Lee, B. Houshmand,
and M. Zimmerman
University of Illinois
Urbana, Illinois

and

R. Acosta
Lewis Research Center
Cleveland, Ohio

May 1989

NASA

A Segmented Mirror Antenna for Radiometers

S.W. Lee.,* B. Houshmand,* and M. Zimmerman*
Electrical and Computer Engineering Department
University of Illinois
Urbana, Illinois 61801

and

R. Acosta
National Aeronautics and Space Administration
Lewis Research Center
Cleveland, Ohio 44135

SUMMARY

The present antenna is designed for the radiometer application on the planned NASA Earth Science Geostationary Platforms in the 1990's. The antenna consists of two parts: a regular parabolic dish of 5 meters in diameter which converts the radiation from feeds into a collimated beam, and a movable mirror that redirects the beam to a prescribed scan direction. The mirror is composed of 28 segmented planar conducting plates, mostly one square meter in size. Based on a physical optics analysis, we have analyzed the secondary pattern of the antenna. For frequencies between 50 and 230 GHz, and for a scan range of ±8° (270 beamwidths scan at 230 GHz), the worst calculated beam efficiency is 95%. To cover such a wide frequency and scan range, each of the 28 plates is individually controlled for a tilting less than 4°, and for a sliding less than 0.5 cm.The sliding is done at discrete steps. At 230 GHz, a step size of 2 mil is sufficient. The plate positions must be reset for each frequency and for each scan direction. Once the position is set, the frequency bandwidth of the antenna is very narrow.

*This work is supported by NASA Grant NAG 3-419.

I. Introduction

A key instrument on the proposed NASA Earth Science Geostationary Platforms (ESGP) is a large radiometer antenna for atmospheric sounding. Even in its "near term" version, the antenna has unprecedented stringent requirements [1], namely,

i) There are 4 to 6 operating frequency bands between 50 to 230 GHz.

ii) The antenna diameter is about 5 meter (833 λ to 3,833 λ)

iii) The beam is to scan $\pm 8^\circ$ for the earth coverage in both azimuthal and elevation planes, corresponding to roughly ± 60 to 270 beamwidth scan.

iii) The beam efficiency, defined by the fractional power in the main beam should exceed 95%.

The above requirements immediately rule out several antenna candidates:

i) Currently space-qualified phase shifters are not available for frequency higher than 20-40 GHz. Even in the next ten years, any beam forming scheme relying on phase shifter is risky.

ii) The 5:1 band makes it impractical to use arrays with discrete radiating elements.

iii) Conventional reflector scan is achieved by feed displacement [2.3]. Such a scan normally has a range of tens of beamwidth, which is one order of magnitude short of the requirement. The use of cluster feed [3,4] for scan compensation again depends on the availability of phase shifters. Furthermore, the degree of compensation is generally not good enough to produce 95% beam efficiency .

We are left with few alternatives, one of which is the mechanically scanned reflector antenna. After all, such an antenna has been the overwhelming choice of existing radiometers [5]. In the ESGP application, however, there is one problem. As a whole,the 5-meter antenna is too large to be moved on a geostationary satellite. If we are able to

segment the reflector surface into smaller pieces, the scan motion may be more manageable. This is the motivation behind our study of a segmented mirror antenna.

The original mirror antenna concept [6-8] can be simply explained below. As sketched in Figure 1,the antenna consists two parts: a regular parabolic dish which converts a spherical wave into a plane wave, and a tilting mirror whose motion redirects the plane wave into a desired scan direction. The advantages of the mirror antenna are as follows:

i) The antenna main beam is always collimated (no aperture phase error) for all scan angles, and for all frequencies.

(ii) The mirror is tilted at an angle θ to obtain a 2θ beam scan. The factor of 2 aids in mechanical motion.

Its disadvantage is that , in addition to the regular parabolic dish, the extra mirror is just as large as or larger than the dish.Tilting the mirror is not any easier than tilting the dish. Hence the mirror antenna in its original form is not suitable for the ESPG application.We propose to segment the mirror into 28 pieces, and move each piece is individually. By so doing, we gain in some mechanical aspects, but we lose in other mechanical as well as some electrical aspects. Does the trade-off pay ? We shall examine this question from an electrical viewpoint, namely, to what extent does the antenna radiation characteristics deteriorate because of the use of 28 small plates instead of a one-piece mirror .The mechanical question of controlling the motion of the plates is not addressed here.

II. Mirror Antenna

The mirror antenna can by symmetrical [8], or offset. In the present application, it must be offset because of the multiple frequency band requirement. An offset mirror antenna is sketched in Figure 1. A regular parabolic reflector is to convert the incoming spherical wave from its feed into a plane wave going in the (-y) direction. A 45°-mirror at position A redirects the plane wave to the +z direction, which in the far field produces the on-axis main beam. To scan the beam to a new direction (θ_0, ϕ_0), the mirror is tilted to a new position B such that the unit normal of surface A, denoted by $\hat{z}_{45}$, moves to $\hat{n}$. Here

$$\hat{n} = \hat{x}\, n_1 + \hat{y}\, n_2 + \hat{z}\, n_3 \tag{2.1}$$

where

$$n_1 = \frac{u_0}{2\, n_2} \quad , \quad n_2 = \sqrt{\frac{1 + v_0}{2}} \quad , \quad n_3 = \frac{w_0}{2\, n_2}$$

$$u_0 = \sin\theta_0 \cos\phi_0 \ , \ v_0 = \sin\theta_0 \sin\phi_0 \ , \ w_0 = \cos\theta_0$$

There are different ways that $\hat{z}_{45}$ can be tilted into $\hat{n}$. We choose the one sketched in Figure 2, namely, $\hat{z}_{45}$ rotates about the $\hat{y}_{45}$ axis by an azimuthal angle AZ, and then moves up by an elevation angle EL, where

$$AZ = \tan^{-1}\left(\frac{\sqrt{2}\, n_1}{n_2 + n_3}\right) \tag{2.2a}$$

$$EL = \sin^{-1}\left[\frac{1}{\sqrt{2}}(n_2 - n_3)\right] \tag{2.2b}$$

Several remarks on the mirror antenna are in order.

(1) When the mirror is at the no-scan position A, the footprint of the incoming plane wave is an ellipse with semi–axes (a, $\sqrt{2}$ a), as shown in Figure 3. Normally, one may choose the mirror slightly oversized to avoid spillover loss at scanning.

(2) Apart from the possible spillover loss mentioned above, there is no scan loss due to phase error.

(3) Both the parabolic reflector and the mirror work for all frequencies. Hence, the limiting factor for the frequency bandwidth is that of the feed. For widely separated frequency bands, we may use frequency selective surfaces as multiplexier to circumvent the feed bandwidth problem. An example is sketched in Figure 4.

(4) To scan the main beam by a polar angle θ_0 from the z-axis, the mirror tilts about $\theta_0/2$. For the ESPG application, a typical dish diameter is 5 meter. When the beam scans ±8° in elevation, the linear motion of the mirror edges is

$$(\pm 4^\circ) \times \frac{\pi}{180^\circ} \times \sqrt{2}\, a = \pm 25 \text{ cm} \tag{2.3}$$

At the intended scan rate for the radiometer, the motion distance in (2.3) is too large to be acceptable for a satellite antenna.

III. Segmented Mirror

The motion of a large (one-piece) mirror presents mechanical problems. To circumvent this difficulty, we propose a segmented mirror, which is made of smaller flat plates. Each plate can be individually controlled for tilting and sliding motions. The segmentation can be done in different ways. An example is shown in Figure 4, where 28 rectangular plates are used. Other plate shapes such as triangles or hexagons may be just as useful. We choose the rectangles for simple analysis (an extension to hexagons are being carried out).

Scanning with the plate mirror is achieved in the manner described below. At the no-scan position, all the plates are aligned on the 45° plane (Figure 5). To scan the beam to the direction

$$\hat{k}^r = \hat{x}\, u_0 + \hat{y}\, v_0 + \hat{z}\, w_0 \tag{3.1}$$

Each plate is undergone two motions:

(1) The plate is tilted to the common direction $\hat{n}$ in (2.1) in the manner sketched in Figure 2.

(2) Along the normal direction to the 45° plane, a typical plate is slid by a distance Δ from its old center position, described by

$$\vec{r}_1 = \hat{x}\, x_1 + \hat{y}\, y_1 + \hat{z}\, (-y_1) \tag{3.2}$$

to a new center position described by

$$\vec{r}_2 = \hat{x}\, x_1 + \hat{y}\left(y_1 + \frac{\Delta}{\sqrt{2}}\right) + \hat{z}\left(-y_1 + \frac{\Delta}{\sqrt{2}}\right) \tag{3.3}$$

The sign of Δ is positive if point 2 is in front of point 1.

The sliding distance Δ is determined by the condition that all the reflected rays from plates must be collimated in the direction $\hat{k}_r$. Referring to Figure 5, we note that the difference in path length between ray 32 and a reference ray 04 is given by

$$\begin{aligned}\delta &= 32 - 04 = (-y_2) - \vec{r}_2 \cdot \hat{k}^r \\ &= (-1)\left[u_0 x_1 + (1 + v_0 - w_0) y_1 + \frac{1}{\sqrt{2}} (1 + v_0 + w_0) \Delta \right]\end{aligned} \tag{3.4}$$

Set the path difference to zero, and the solution of Δ from (3.4) is

$$\Delta_{optical} = \frac{-\sqrt{2}}{1+ v_0 + w_0} [u_0 x_1 + (1 + v_0 - w_0) y_1] \tag{3.5}$$

The subscript "optical" signifies the fact that, when (3.5) is satisfied, rays are collimated in the $\hat{k}_r$ direction for all frequencies. It is a simple matter to show that by sliding a distance $\Delta_{optical}$, point 1 is moved to point 5, which is on the plane BB'. Then the plate mirror becomes the one-piece mirror sketched in Figure 1, which, of course, is not the case of interest.

Now, for a fixed frequency, we may set δ in (3.4) to a multiple of wavelengths, and still maintain the perfect beam collimation. Thus, alternative solutions of Δ are

$$\Delta = \frac{-\sqrt{2}}{1+ v_0 + w_0} [u_0 x_1 + (1 + v_0 - w_0) y_1 + m \lambda] \tag{3.6}$$

where $m = 0, \pm 1, \pm 2, \ldots$. We choose m to obtain a minimum $|\Delta|$.

Let us summarize our results. Point 1 at $(x_1, y_1, z = -y_1)$ is the center point on a plate lying on the 45° plane (Figure 5). In order to scan the beam in the direction of $\hat{k}_r$ in (3.1). The plate must be tilted to the new direction $\hat{n}$ in (2.1), and slided by a distance Δ in (3.6). Then the reflection from the plate produces a perfectly collimated beam in direction $\hat{k}_r$.

The use of Δ in (3.6), instead of that in (3.5), allows us to slide each plate by a very small distance. As a consequence, the mechanical problem of one-piece mirror is circumvented. The price that we paid, of course, is that the mirror works only for a given frequency. For wide band applications, we must slide each plate to a new position for each new frequency in a time sharing manner.

The linear motion of the plate edge due to tilting is also reduced because the plate size is smaller. For the 28-plate mirror in Figure 4, the largest plate has a dimension of 0.2a instead of a. Consequently, the maximum linear motion is reduced by a factor of 5 (i.e., 5 cm instead of 25 cm; described in (2.3)).

Let us consider the possible phase error over the antenna aperture (or individual plate) due to scan. If a plate is slid by the $\Delta_{optical}$ in (3.5), there is no phase error. In order to reduce the distance of sliding, we use Δ in (3.6) instead. As long as there is only a fixed frequency, there is still no phase error. The range of Δ is within $\pm\Delta_{max}$, where

$$2\Delta_{max} = \frac{\sqrt{2}\,\lambda}{1 + \cos\theta_0 - |\sin\theta_0|} \tag{3.7}$$

The above sliding range is plotted as a function of frequency and scan angle in Figure 7. For scan up to $\pm 8°$ at 50 GHz, the range is 0.46 cm, or 180 mils. Mechanically, it is desirable to have discrete, instead of continuous sliding. Analogous to the term used on phase shifters, an N-bit sliding has 2^N steps in the range given in (3.7). Commonly, a 4-bit sliding (16 steps) is adequate. For a fixed sliding step d, the maximum possible phase error is given by

$$\text{Max. phase error} = 127° \left(1 + \cos\theta_0 + |\sin\theta_0|\right) \frac{d}{\lambda} \tag{3.8}$$

which is plotted in Figure 8. To avoid high sidelobes, the phase error is usually kept within 11° (corresponding to a 4-bit phase shifter). For scan up to $\pm 8°$ at 230 Ghz, the sliding step

should not exceed 2.4 mils.We choose 2 mils a step in our later calculations. In summary, phase error for the present antenna arises from

(i) operation at a frequency which deviates from the designed frequency

(ii) sliding of the plates is discrete at a predetermined step instead of continuous.

In Section V, we shall examine the effect on antenna patterns due to the phase error.

A remark on segmentation is in order. Segmentation of a large antenna into smaller pieces has been known and practiced for a long time[9,10]. If a doubly curved reflector is segmented into flat plates, phase error is present with or without scan. A high beam efficiency antenna can not be achieved in such a way. Our segmentation does not have this phase error problem at all, because our reflector (mirror) is flat to begin with. This price we paid of course is to have an extra parabolic dish.

IV. Antenna Secondary Pattern Computation

To calculate the antenna secondary pattern, we apply the standard physical optics (PO) theory by integrating the induced PO current on all plates. To this end, it is convenient to introduce the local plate coordinate for each plate (Figure 6). The center of the plate coordinate is at point 2, which is described in (3.3). The base vectors of the plate coordinates are $(\hat{x}'_{45}, \hat{y}'_{45}, \hat{z}'_{45} = \hat{n})$. By choosing the tilting motion described in Figure 2, we find

$$\begin{bmatrix} \hat{x}'_{45} \\ \hat{y}'_{45} \\ \hat{z}'_{45} \end{bmatrix} = \overline{\overline{T}} \begin{bmatrix} \hat{x} \\ \hat{y} \\ \hat{z} \end{bmatrix} \tag{4.1}$$

where matrix $\overline{\overline{T}}$ has elements

$$t_{11} = s_1 \quad , \; t_{12} = \frac{(s_3 + s_2)}{\sqrt{2}} \quad , \; t_{13} = \frac{(s_3 - s_2)}{\sqrt{2}}$$

$$t_{21} = s_4 \quad , \; t_{22} = \frac{(s_6 + s_5)}{\sqrt{2}} \quad , \; t_{23} = \frac{(s_6 - s_5)}{\sqrt{2}}$$

$$t_{31} = s_7 \quad , \; t_{32} = \frac{(s_9 + s_8)}{\sqrt{2}} \quad , \; t_{33} = \frac{(s_9 - s_8)}{\sqrt{2}}$$

$$s_1 = \cos(AZ) \quad , \; s_2 = 0 \quad , \; s_3 = -\sin(AZ)$$

$$s_4 = -\sin(EL)\sin(AZ) \quad , \; s_5 = \cos(EL) \quad , \; s_6 = -\sin(EL)\cos(AZ)$$

$$s_7 = \cos(EL)\sin(AZ) \quad , \; s_8 = \sin(EL) \quad , \; s_9 = \cos(EL)\cos(AZ)$$

(AZ, EL) given in (2.2)

Before tilting and sliding, let a typical point on the plate be denoted by a in Figure 7, and is described by a position vector in the main coordinate

$$\vec{r}_a = \hat{x}\, x_a + \hat{y}\, y_a + \hat{z}\, z_a \tag{4.2}$$

After tilting and sliding, the same point on the plate is now located at position b described by

$$\vec{r}_b = \hat{x}\, x_b + \hat{y}\, y_b + \hat{z}\, z_b \tag{4.3}$$

It can be shown that

$$\begin{bmatrix} x_b \\ y_b \\ z_b \end{bmatrix} = \bar{\bar{T}}^T \begin{bmatrix} x_a - x_1 \\ y_a - y_1 \\ 0 \end{bmatrix} + \begin{bmatrix} x_a \\ (y_a + \Delta)/\sqrt{2} \\ (-y_a + \Delta)/\sqrt{2} \end{bmatrix} \tag{4.4}$$

Here $(x_1, y_1, 0)$ is the coordinator of center point 1. Matrix $\bar{\bar{T}}$ is given in (4.1), and the subscript T is the transpose operator.

In the present pattern computation, we ignore part of the beam waveguide analysis. The feed is simply modelled by a point source located at the total point F of the parabolic reflector (Figure 1). The patterns in the E-plane, and H-plane are, respectively,

$$(\cos\theta_f)^{QE}, \text{ and } (\cos\theta_f)^{QH} \tag{4.5}$$

when θ_f is the polar angle in the feed coordinates. It is known that (4.5) is a good approximation for common scalar feed horns used in radiometer applications. We trace the geometrical optic rays from the feed through the parabolic reflector, and then to a typical plate, which has been tilted and slid to the correct position for scanning. According to PO, the induced current on the plate is

$$\vec{J}_s = 2\, \hat{n} \times \vec{H}^i \tag{4.6}$$

Next, we integrate the above current over all plates to calculate the antenna secondary pattern. In this step, results in (4.1) and (4.4) are used.

In the radiometer application, the important parameter is the beam efficiency e. Consider the antenna in transmitting mode(Figure 1), e is defined by

$$e = \frac{P_{beam}}{P_{feed}} \tag{4.7a}$$

where

$$P_{feed} = \text{total power radiated from the feed} \tag{4.7b}$$

$$P_{beam} = \text{power in the reference polarization in the main beam} \tag{4.7c}$$

The extent of the ' main beam' has been customarily defined as [4, p22-27]:

i) the null to null beamwiths, or

ii) "the 2.5 times half-power beamwidth".

Definition ii) is particularly useful in measured patterns where the null may not be easily identifiable. In this paper, we use definition i).

For a beam on the boresight of the antenna ($\theta_0 = 0°$ in Figure 1), the pattern is azimuthally symmetrical, and there is no ambiguity in applying (4.7). Let us denote the half null-to-null beamwidth by θ_{null}. However, as the beam scans to a new direction (θ_0, ϕ_0), the symmetry is lost, and the null-to-null width varies in different pattern cuts. Then, instead of using (4.7c), we define

$$P_{beam} = \text{power within a cone around the main beam direction } (\theta_0, \phi_0), \tag{4.8}$$
$$\text{with the half cone angle equal to } \theta_{null} \text{ obtained in the no-scan case}$$

The present pattern computation is based on PO described in (4.6). It is known that power conservation does not hold within the PO theory. In other words, if one integrates the antenna secondary pattern over the 4π radian space, the resultant power does not in gerenal equal to the incident power interceped by the reflector. For this reason, one has to be careful in calculating the beam efficiency.

For the reason just explained, a direct evaluation of (4.7a) for scanned cases often leads to inaccurate results. We use an indirect evalution , namely,

$$e = e_{spill} * e_{miss} * e_{block} * e_{pat} \tag{4.9}$$

where (Figure 1)

e_{spill} = fractional of the incident feed power intercepted by the parbolic dish (counting the spilloever loss).

e_{miss} = fractional of the incident power from the parabolic dish intercepted the elliptcal mirror (counting the incident power missing the mirror).

e_{block} = fractional of the power received by the mirror but not blocked by the feed (counting the power blocked by the feed).

e_{pat} = fractional of power in the secondary pattern confined in the main beam.

Ideally, e_{pat} should be the ratio of the p_{beam} in (4.8) and p_{pat}, which is the total radiated power in the secondary pattern in the 4π radian space. Unfortunately, p_{pat} cannot be readily calculated. The reasons are as follows:

(i) Any PO-based pattern computation method gives accurate pattern result only in the angular region near the main beam. Means for calculating far-out lobes exist, such as adding fringe currents, using edge diffraction, etc. Their implementation is difficult, and may not be worthwhile.

(ii) In practical antennas, far-out lobes are mostly affected by supporting struts, and near-by structures. Patterns calculated from models do not include those factors and are not realistic.

(iii) For radiometers, far-out lobes usually point to a cold environment. Whether their power is included in p_{pat} is often not critical.

In the present analysis, we approximate p_{pat} by p_{pat} (approx), where

p_{pat} (approx) = power within a cone around the main beam direction (θ_0, ϕ_0), with the half cone angle equal to $10^* \theta_{null}$, instead of the 4π radian space.

As explained earlier, θ_{null} is the half null-to-null beamwidth in the no-scan case.

V. Numerical Results

For numerical results, we consider the ESPG radiometer antenna specified in Section I. The parameters of the antenna are chosen as follows (Figure 1):

a = parabolic dish diameter = 5m

f = focal length of the dish = 2 m, which makes f / D = 0.4

d = discrete sliding step size of the mirror = 2 mils

QE = QH = feed pattern index defined in (4.5) = 2.0, which results in 17 dB edge taper in the reflector aperture.

Polarization is horizontal (E_x in the mirror aperture)

Results are summaried below.

i) **Boresight patterns.** For the no-scan case, the patterns for the lowest and the highest frequencies are plotted in Figures 9 and 10. Even with discrete sliding, there is no phase error in the mirror aperture. Hence, the pattern is smooth and sharp nulls. Sidelobes are lower than -30 dB.

ii) **Scanned Patterns.** When the beam scans, effects of both mirror segmentation and the sliding discretization come in. The worst case occurs at the highest frequency and the extreme scan angle. Patterns are shown in Figures 11 and 12. The sidelobe level is at 24 dB. In the $\phi_0 = 90°$ scan (downward scan), the pattern is characterized by grating lobe effect due to the segmentation, i.e. lobes at $\theta = 7.91°$, 8.09°, etc. The 2-mil step raises the near-in sidelobes and fills in the nulls as expected.

iii) **Beamwidth and Null Position.** For the boresight beam, the results are shown in Figure 13. Those calculated results fit approximately the following formula:

$$\text{3 dB Beamwidth} \approx 105° \lambda / D \tag{5.1}$$

$$\text{Null to Null Beamwidth} \approx 148° \lambda / D \tag{5.2}$$

It follows that

Null to Null Beamwidth ≈ K * (3 dB Beamwidth) (5.3)

where K= 1.4. These formulas are valid for the present -17 dB edge taper, which is typical for radiometer antennas. The usual definition of " 2.5 times half-power beamwidth " [4] for the approximated null to null beamwidth appears to mean K= 2.5 / 2 = 1.25.

iv) **Power Distribution.** Around the main beam, a cone is defined. The percentage of total radiated power from the feed within the cone is plotted in Figures 14 and 15 for two 230 GHz cases. The losses attributed to spillover, feed blockage, and possible missing of the mirror is less than 2% of power. The rest of power is mostly confined in the main beam, even for the 8° scan case.

v) **Beam Efficiency.** We plot beam efficiency as a function of scan angle in the diagonal plane ($\phi_0 = 45°$). Except for the boresight beam, the efficiency in an average sense increases with the decreasing sliding step size and therefore the aperture phase error. The phase error is of the 'hit or miss' nature, which explains the uneven variation of the curves. At 230 GHz, the 95% efficiency can be met with a 2 mil step size, which is 1/26 of wavelength. At 50 GHz, the same is met with a 10 mil step (1/ 24 wavelength).

vi) **Frequency Bandwidth Without Resetting Mirror Positions.**Once the mirror position is set for a center frequency, the antenna has a very narrow bandwidth. This is due to the fact that segmentation destroys the equal-path-length condition. In Figure 18, we show a 4° scanned pattern under the condition that the mirror is set for 230 GHz, but the antenna is operated at 227 GHz. The beam is shifted by about 2 beamwidths. The directivity is lowered by 3 dB, and sidelobe is increased significantly. In Figures 19 and 20, we show the beam efficiency for a band of operating frequency. The center frequencies are 50 and 230 GHz, respectively. The rapid degradation in efficiency is due to shift in the main beam away from the the cone defined around the desired scan angle. The 95% beam efficiency can be maintained for ±0.4 GHz at 4° scan, and for ±0.2 GHz at 8° scan.

VI. Conclusion

The radiation pattern of a segmented mirror antenna has been analyzed by a PO theory. The antenna is capable of maintaining 95% beam efficiency over the a wide frequency and scan range.The scan is achieved by tilting and sliding the mirror within a very small range. As far as the electric performance is concerned, the antenna appears to be a viable candidate for the ESGP.

The possible 'show stopper' may come from the required precision control of the segmented mirror. Specifically, in a space environment,

i) can the mirror be moved in an increment of 0.01° tilting for one beamwidth scan, and 2 mil sliding for a maximum 11° phase error ?

ii) can the above motion be done fast enough to meet the required scan rate?

These questions remain to be answered[1].

Other than ESPG, the segmented mirror antenna is a useful antenna in its own right. Especially when the operating frequency is not as high as 230 GHz, the mechanical precision problem is eased.

[1]According to Dr. Craig Rogers of Virginia Polytechnic Institute and State University, requirement i) appears to be feasible.

References

[1] A. J. Gasiewski and D. H. Staelin, "Science requirements for passive microwave sensors on Earth Science Geostationary Platforms", paper presented at NASA Technology Workshop for Earth Science Geostationary Platforms, NASA Langley Research Center, Hampton, Virginia; September 21-22, 1988.

[2] Y. Rahmat-Samii,"Reflector antennas," Chapter 15, *Antenna Handbook Theory Applications and Design*, eds. Y. T. Lo and S. W. Lee, New York: Van Nostrand Reinhold, 1988.

[3] M. Zimmermann, S. W. Lee, R. Rahmat-Samii, B. Houshmand, and R. Acosta, "A comparison of reflector antenna designs for wide-angle scanning," paper presented at NASA Technology Workshop for Earth Science Geostationary Platforms, NASA Langley Research Center, Hampton, Virginia; September 21-22, 1988.

[4] R. Acosta, "Active feed array compensation for reflector antenna surface distortion," Technical Report TM-100826, NASA Lewis Research Center, Cleveland,OH, June 1988.

[5] J. C. Shiue and L. R. Dod,"Remote sensing and microwave radiometry," Chapter 22, *Antenna Handbook Theory Applications and Design*, eds. Y. T. Lo and S. W. Lee, New York: Van Nostrand Reinhold, 1988.

[6] B. L. Lewis and J. P. Shelton, "Mirror scan antenna technology," *IEEE International Radar Conference Record*, April 1980, pp. 279-283.

[7] D. D. Howard and D. C. Cross, " Mirror antenna dual-band lightweight mirror design," *IEEE Trans. Antennas and Propagation*, vol. AP-35, pp. 286-294, March 1985.

[8] D. C. Cross, D. D. Howard, and J. W. Titus, "Mirror-antenna radar concept," *Microwave J.* pp. 323-335, May 1986.

[9] S. Dasgupta and Y. T. Lo, " A study of the coma-corrected zoned mirror by diffraction theory," *IEEE Trans. Antennas and Propagation*, vol. AP-11, pp. 130-139, March 1961.

[10] A. C. Schell, "The multiplate antenna," *IEEE Trans. Antennas and Propagation*, vol. AP-16, pp. 550-560, Sept. 1966.

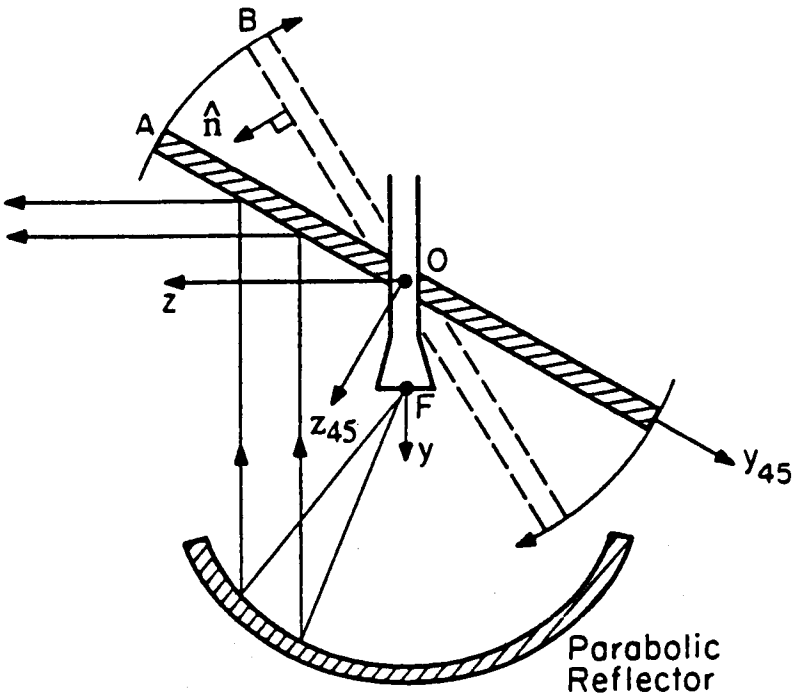

Figure 1. A conventional mirror antenna. The mirror plate is normally at position A to produce an on-axis beam ($\theta_0 = 0$), and is tilted about point 0 for beam scanning.

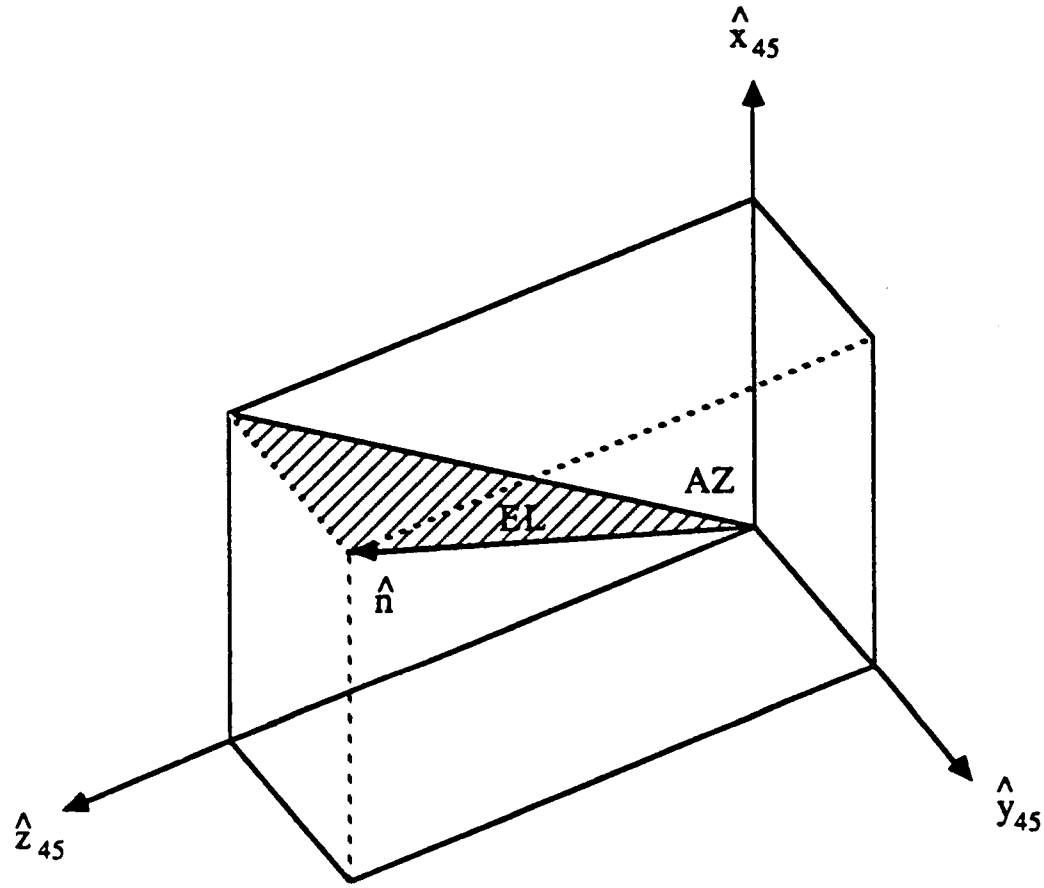

Figure 2. For no-scan case, the normal of the mirror is in the direction $\hat{z}$. To scan the beam, the normal is tilted to the new direction $\hat{n}$. The tilting is done first in the azimutual and then the elevation direction.

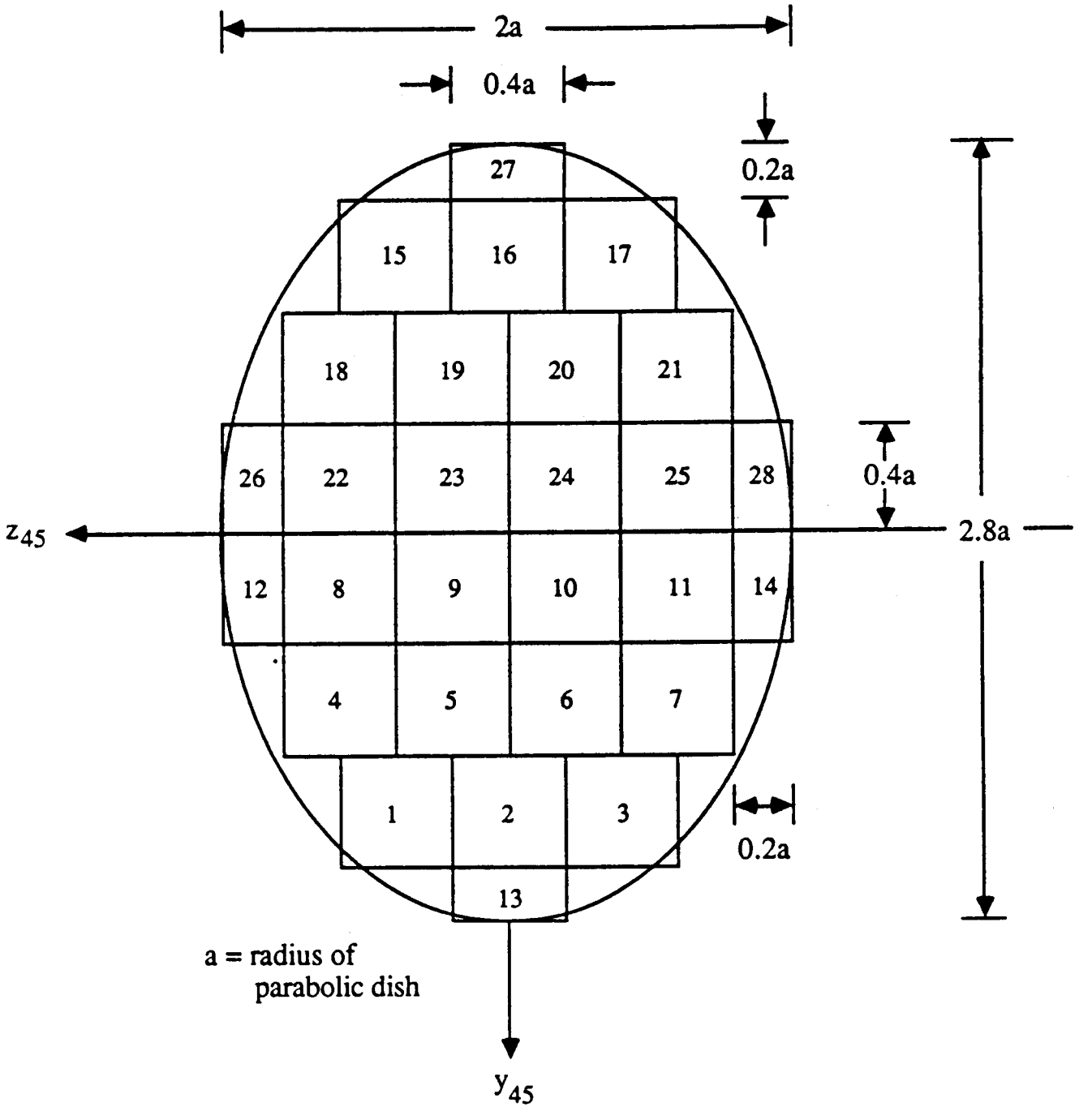

Figure 3. The elliptical mirror is divided into 28 rectangular plates, which can be individually controlled for tilting and sliding.

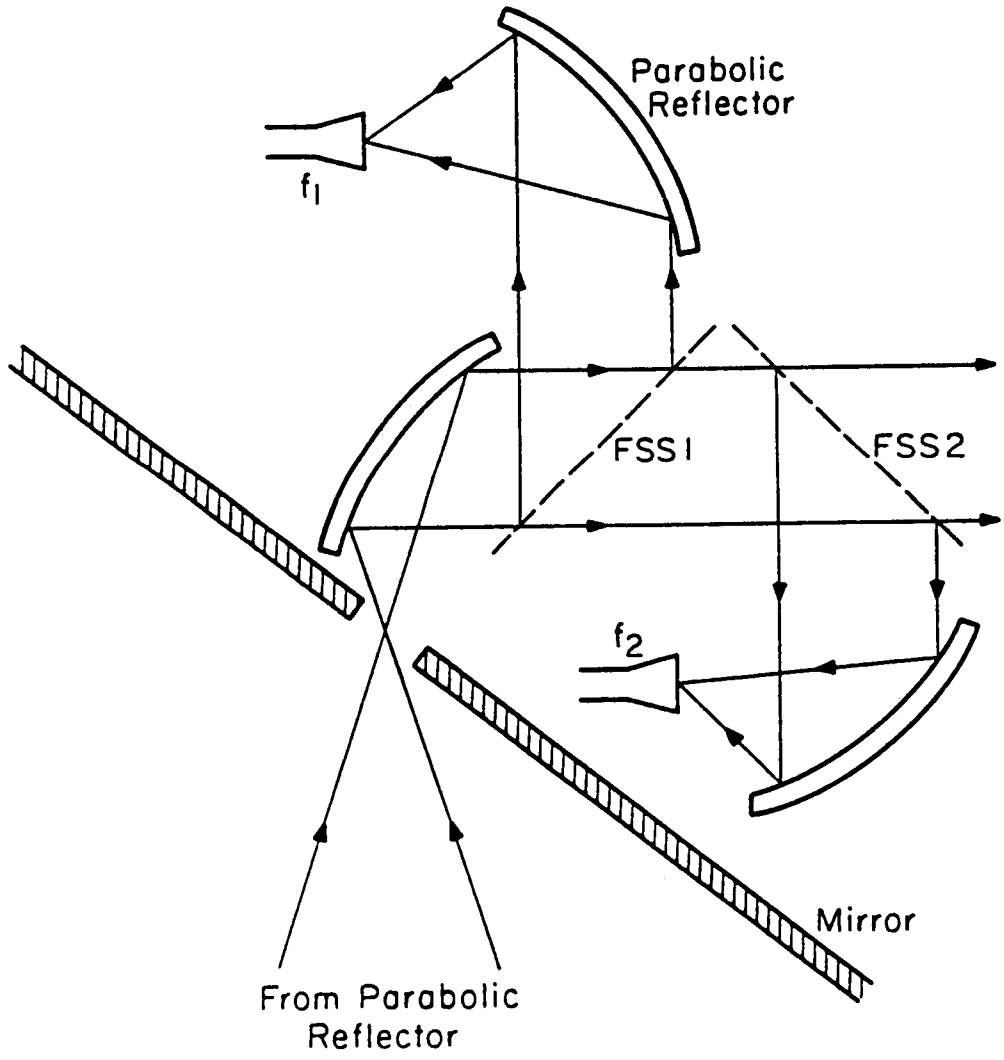

Figure 4. Multiple feeds for different frequency bands can be arranged with beam waveguides, and frequency selective surfaces.

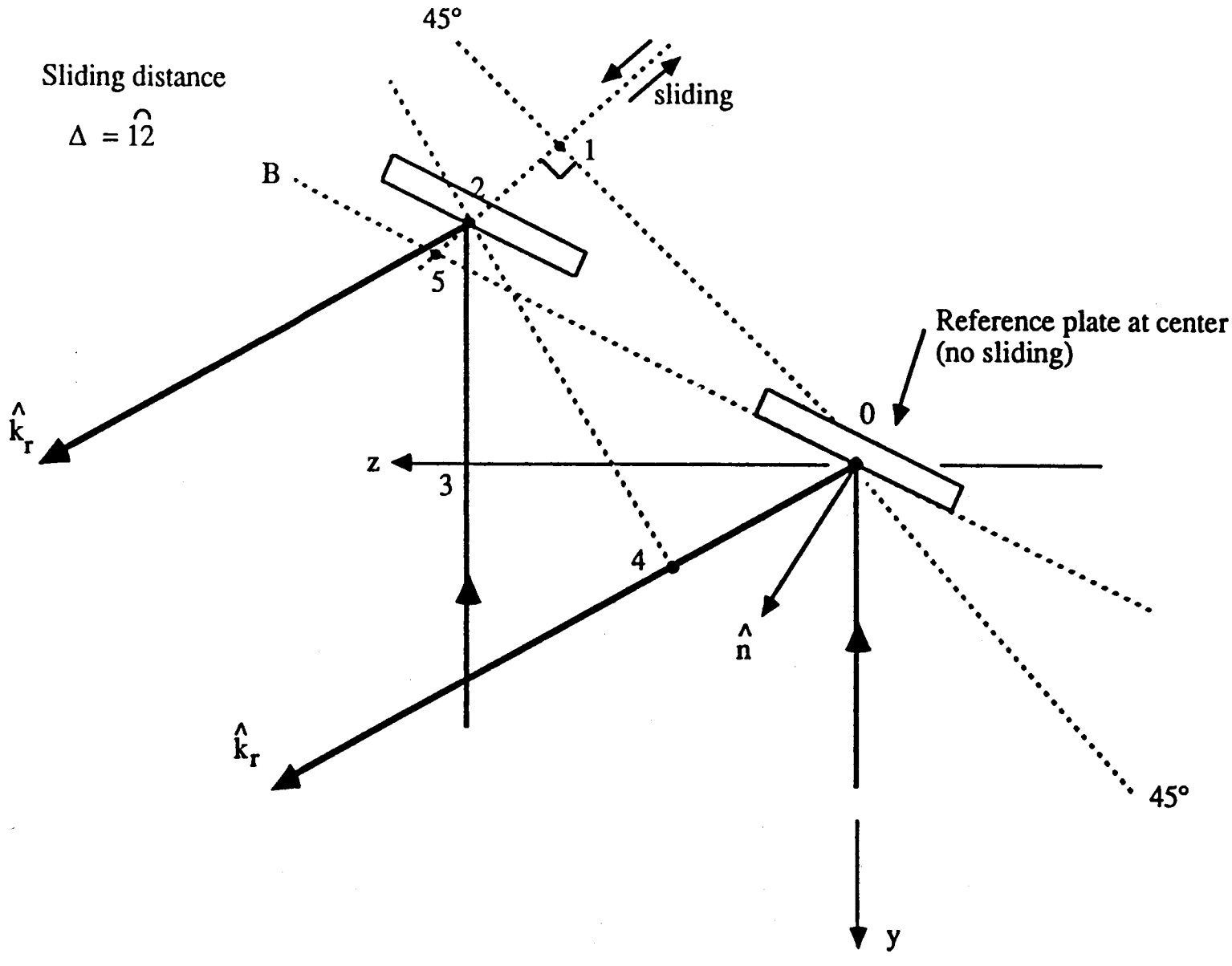

Figure 5. To scan the beam with the plate mirror, a typical plate is tilted to the common direction $\hat{n}$ given in (2.1), and is slid from point 1 to point 2.

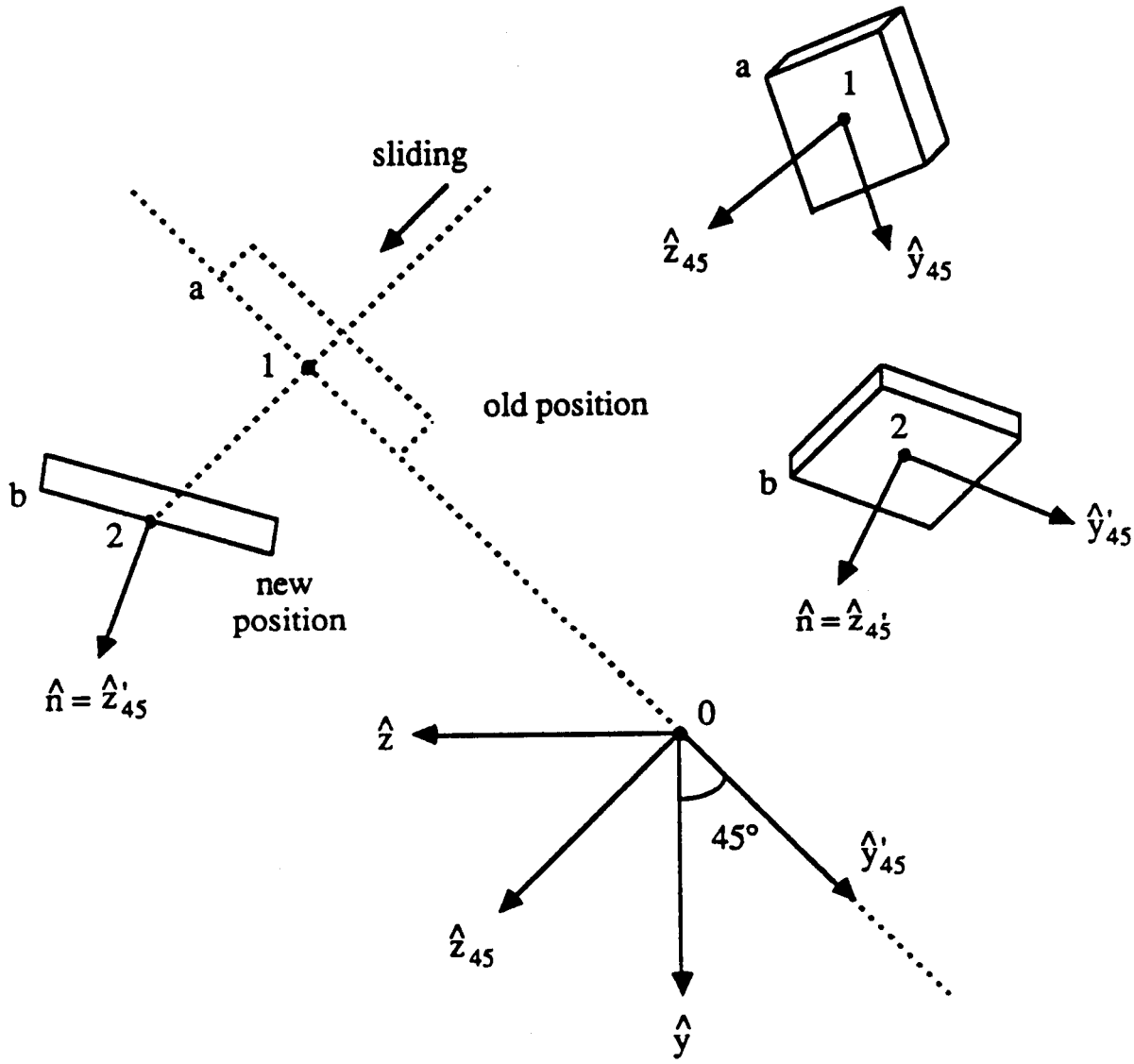

Figure 6. Main coordinate with base vectors $(\hat{x}, \hat{y}, \hat{z})$ centered at 0. For plate 2 at its new position, we introduce the local plate coordinate with base vector $(\hat{x}'_{45}, \hat{y}'_{45}, \hat{z}'_{45} = \hat{n})$.

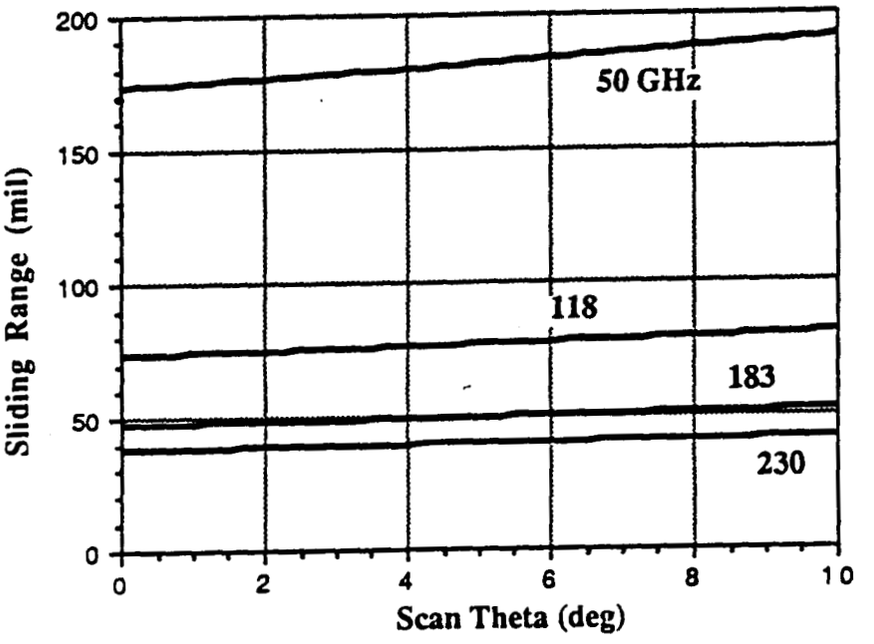

Figure 7. Sliding range as a function of scan angle calculated from Equation (3.7)

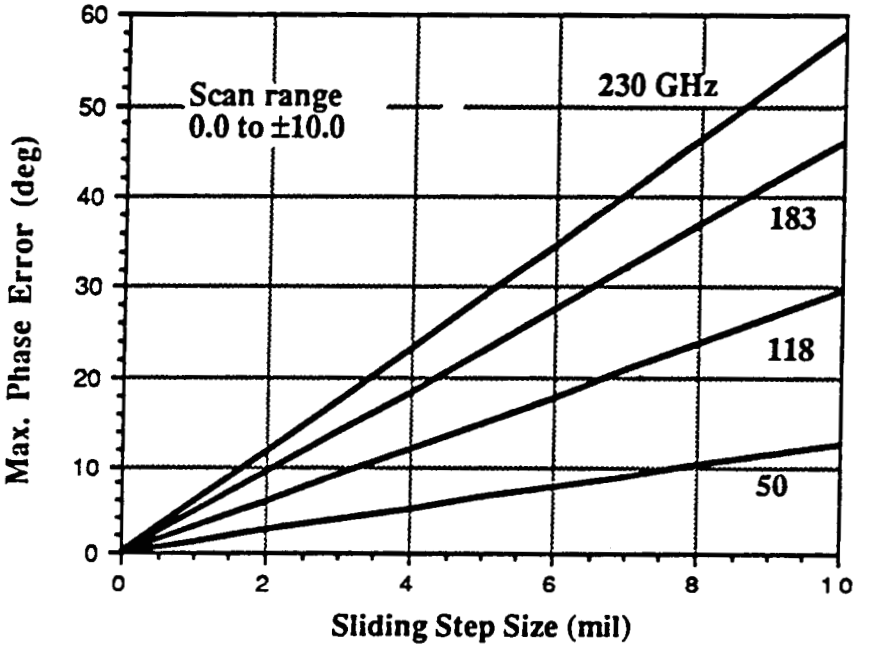

Figure 8. Maximum phase error in the mirror aperture due to the discretization of sliding.

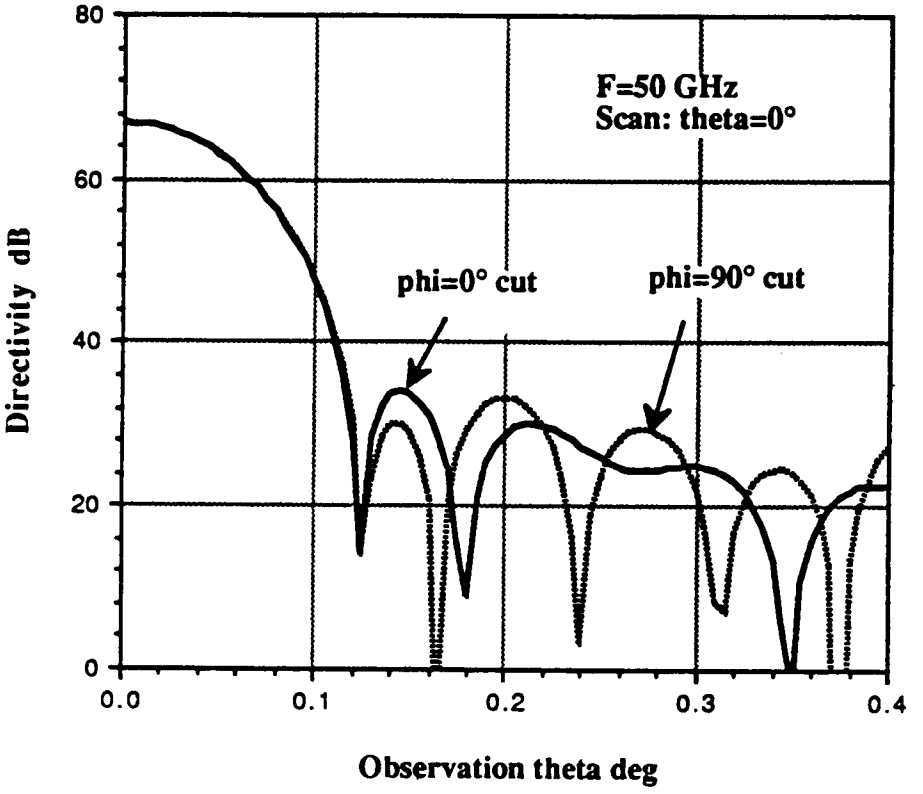

Figure 9. Secondary pattern of the segmented mirror antenna in the no-scan case. F = 50 GHz. Phi = 0° is the E-plane.

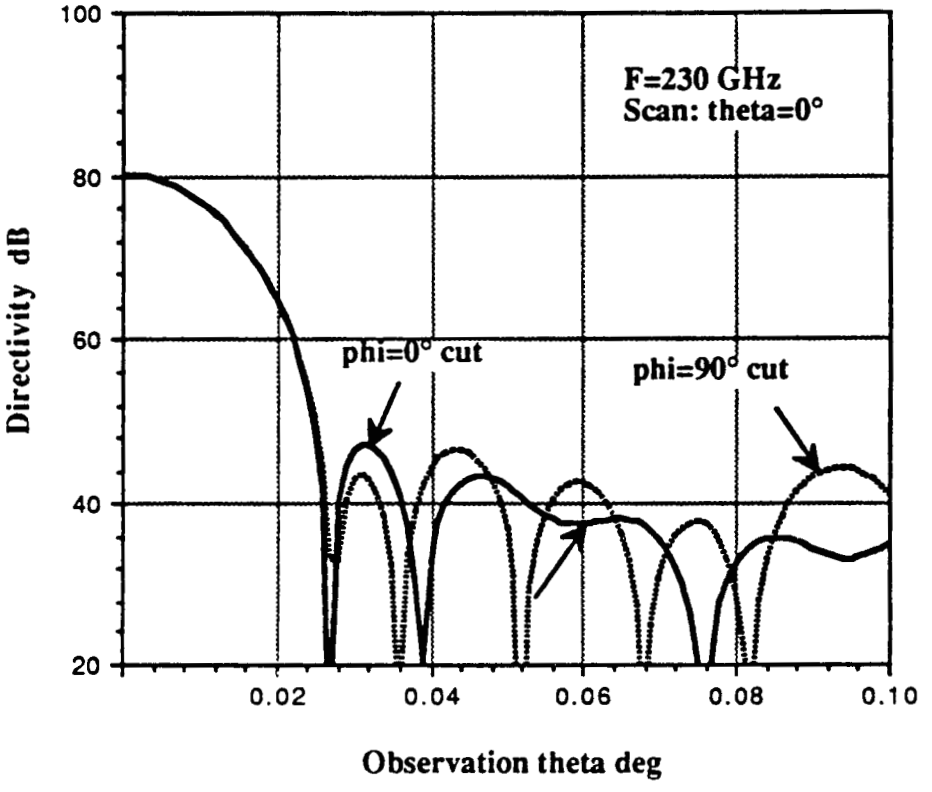

Figure 10. Same as Figure 9 except F = 230 GHz.

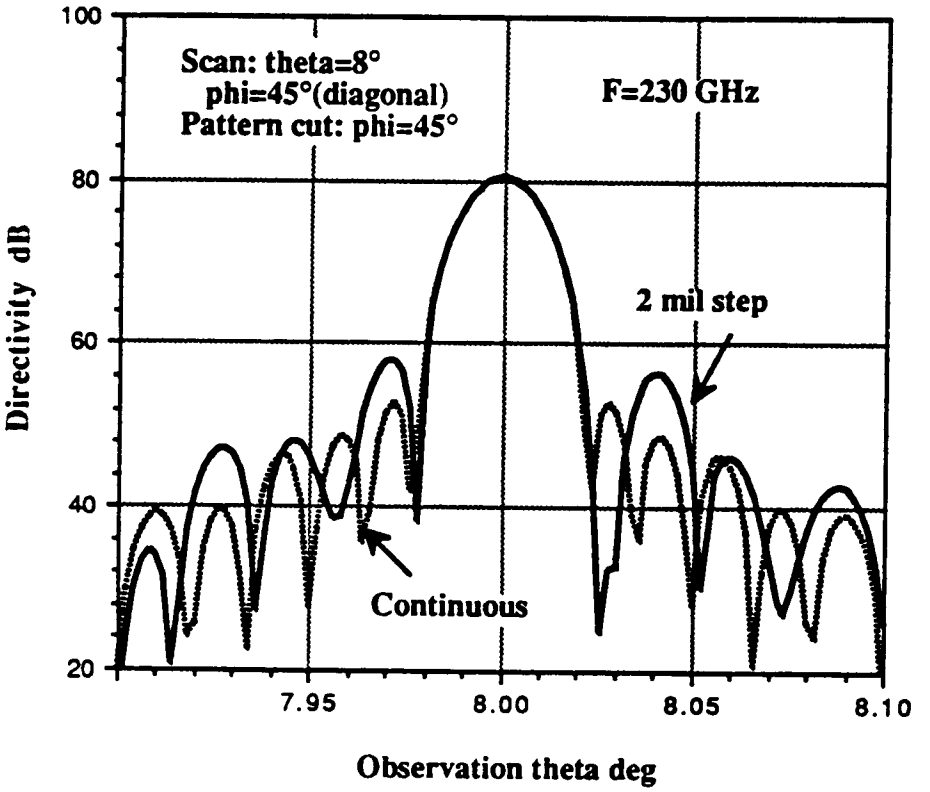

Figure 11. Secondary pattern of the segmented mirror antenna when the beam scans to ($\theta_0 = 8°$, $\phi_0 = 45°$). Mirror plates sliding is either continuous or at 2-mil a step.

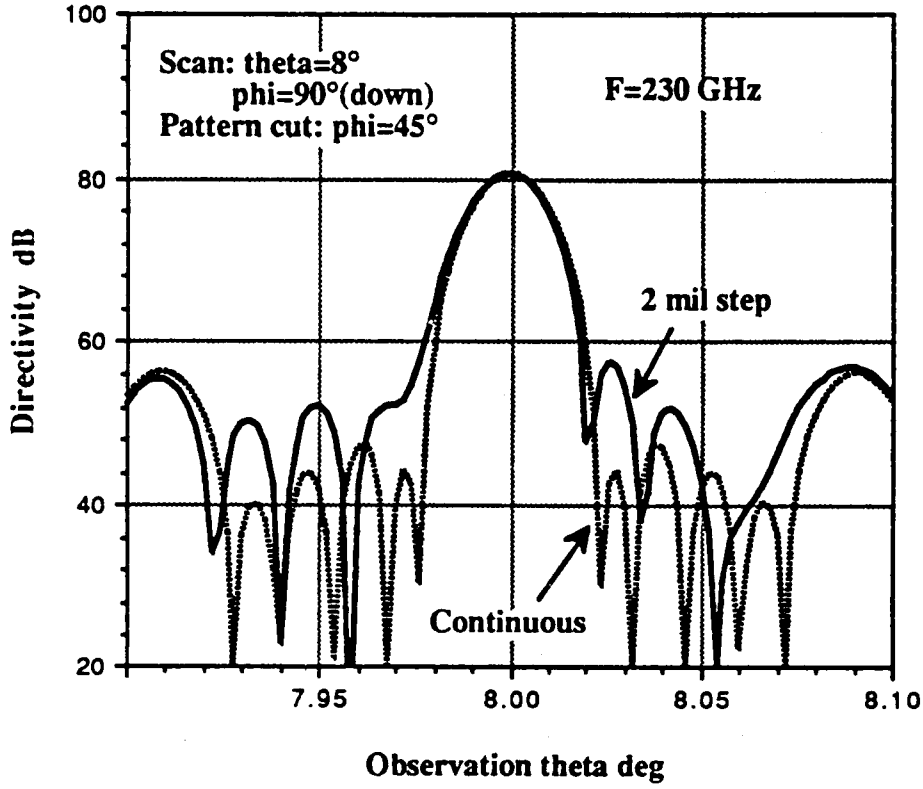

Figure 12. Same as Figure 11 except the beam scans.

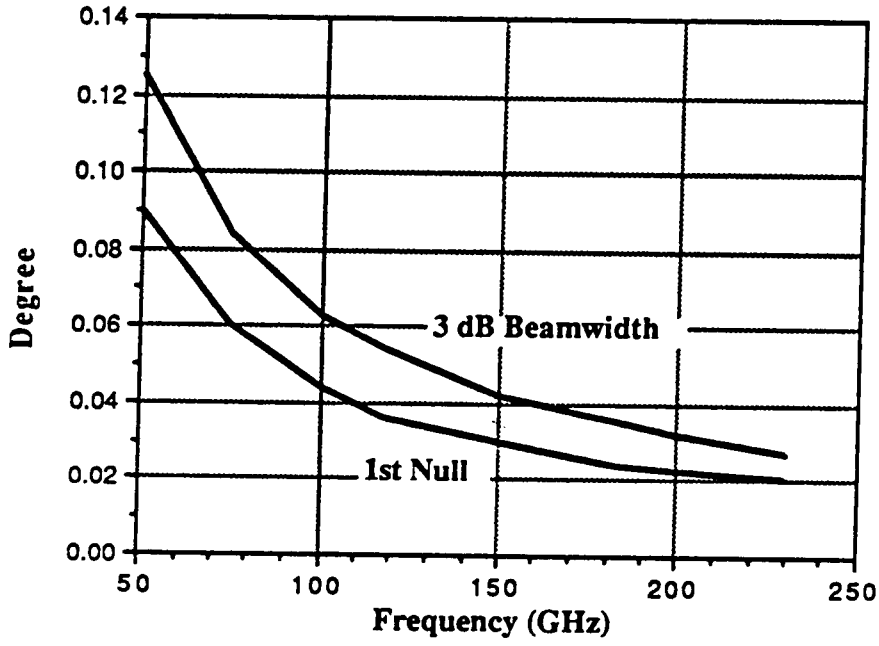

Figure 13. Beamwidth and the first null position for the boresight beam ($\phi_0 = 0°$).

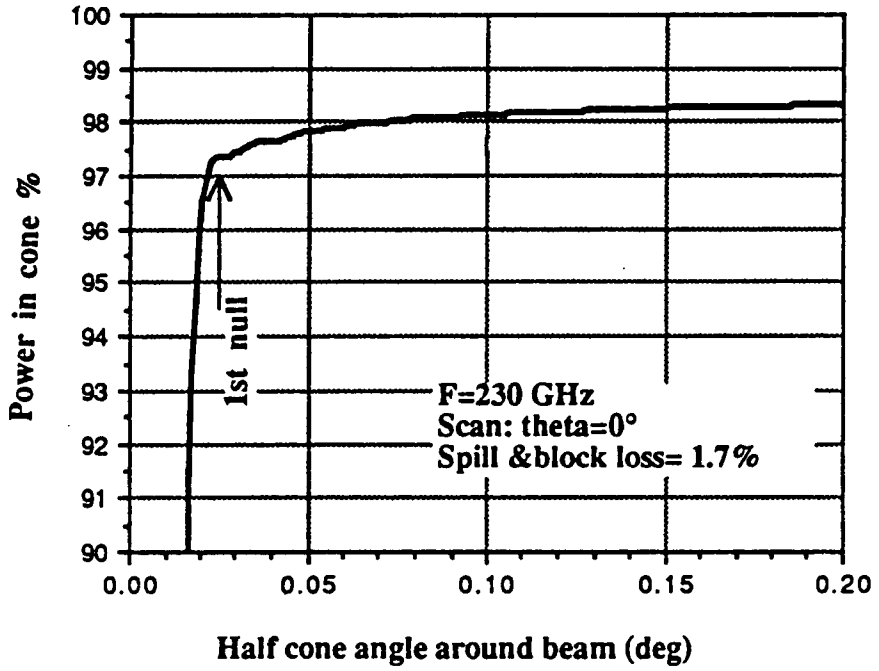

Figure 14. Percentage of power in a cone around the main beam normalized by the total power radiated from the feed.

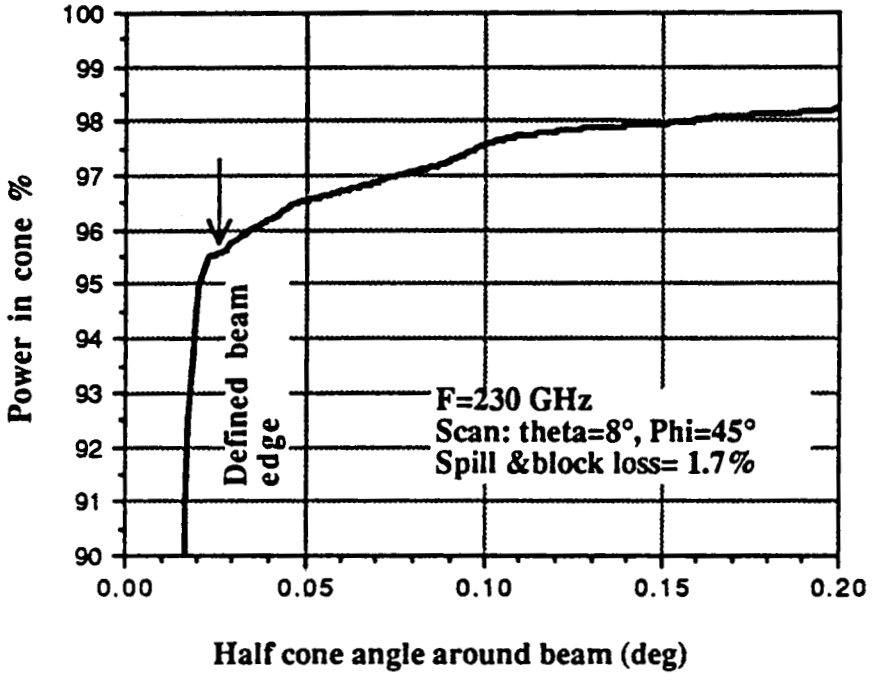

Figure 15. Same as Figure 14 except the beam is at ($\theta_0 = 8°$, $\phi_0 = 45°$). The sliding step size is 2 mils.

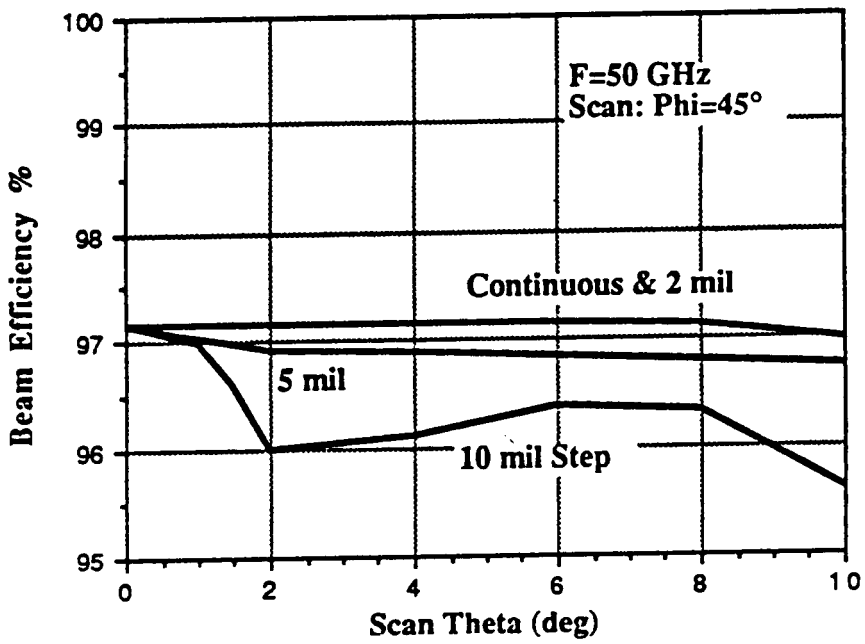

Figure 16. Beam efficiency as a function of scan angle in the diagonal plane for different sliding step sizes. F = 50 GHz. Because the phase error due to discrete sliding is of 'hit and miss' nature, the curves are not monotonic.

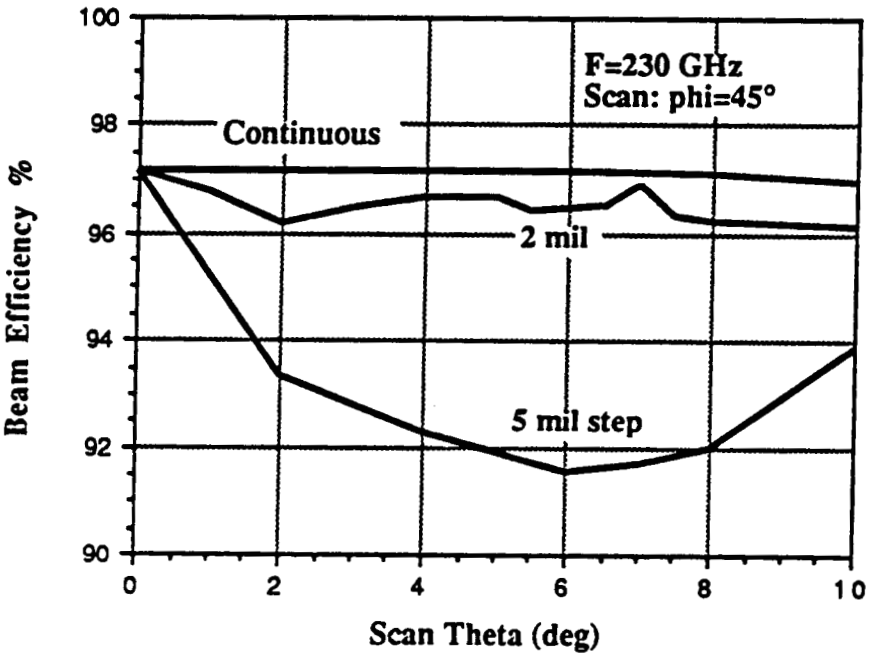

Figure 17. Same as Figure 16 except F = 230 GHz.

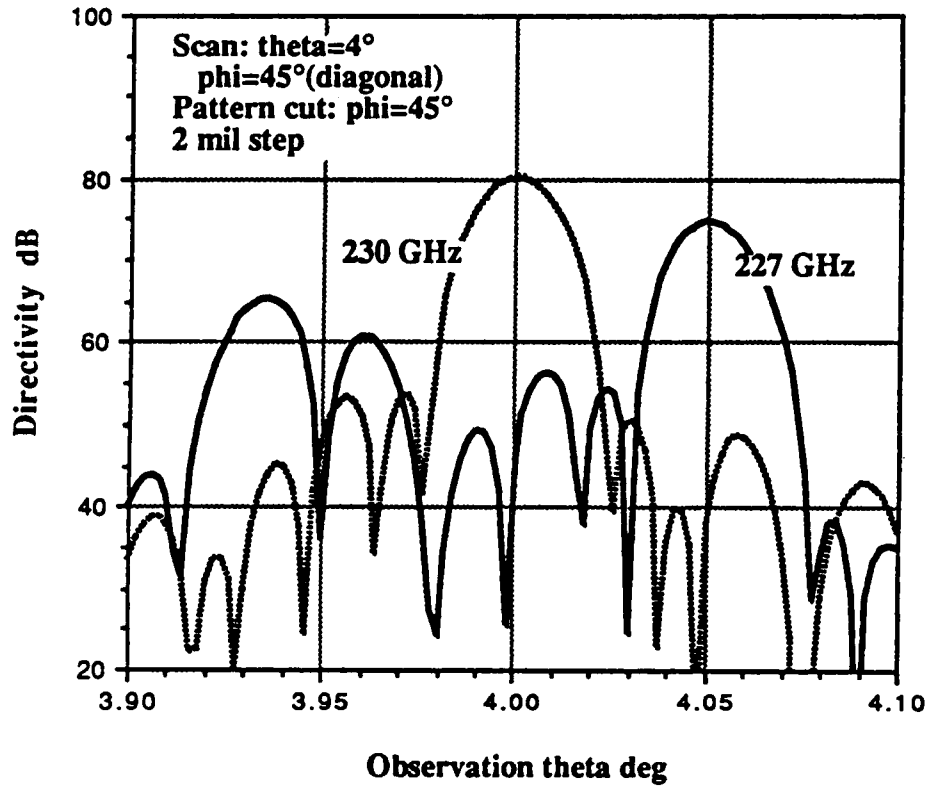

Figure 18. In the diagonal plane, 4° scanned secondary patterns at the central frequency 230 GHz, and at a nearby frequency 227 GHz. The mirror position is set for the central frequency.

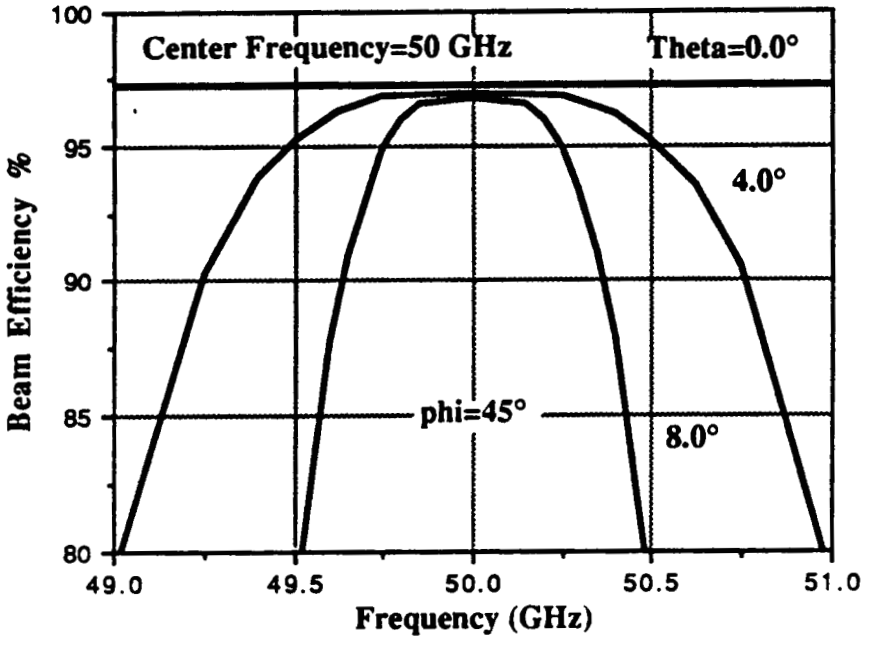

Figure 19. Beam efficiency of the segmented mirror antenna as a function of frequency. The plate position is set for F = 50 GHz.

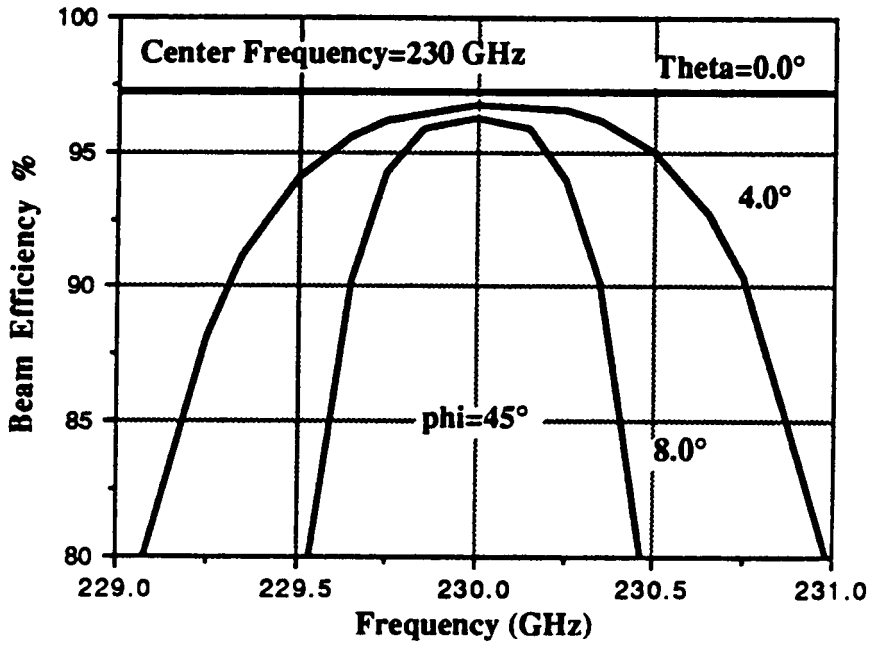

Figure 20. Same as Figure 19 except F = 230 GHz.

NASA
National Aeronautics and Space Administration

Report Documentation Page

1. Report No.	2. Government Accession No.	3. Recipient's Catalog No.
NASA TM-102045 SWL89-2		

4. Title and Subtitle	5. Report Date
A Segmented Mirror Antenna for Radiometers	May 1989
	6. Performing Organization Code

7. Author(s)	8. Performing Organization Report No.
S.W. Lee. B. Houshmand, M. Zimmerman, and R. Acosta	E-4793
	10. Work Unit No. 650-60-20

9. Performing Organization Name and Address	11. Contract or Grant No.
National Aeronautics and Space Administration Lewis Research Center Cleveland, Ohio 44135-3191	13. Type of Report and Period Covered Technical Memorandum
12. Sponsoring Agency Name and Address	14. Sponsoring Agency Code
National Aeronautics and Space Administration Washington, D.C. 20546-0001	

15. Supplementary Notes

S.W. Lee, B. Houshmand, and M. Zimmerman, Electrical and Computer Engineering Department, University of Illinois, Urbana, Illinois 61801 (work funded under NASA Grant NAG3-419); R. Acosta, NASA Lewis Research Center.

16. Abstract

The present antenna is designed for the radiometer application of the planned NASA Earth Science Geostationary Platforms in the 1990's. The antenna consists of two parts: a regular parabolic dish of 5 meters in diameter which converts the radiation from feeds into a collimated beam, and a movable mirror that redirects the beam to a prescribed scan direction. The mirror is composed of 28 segmented planar conducting plates, mostly one square meter in size. Based on a physical optics analysis, we have analyzed the secondary pattern of the antenna. For frequencies between 50 and 230 GHz, and for a scan range of $\pm 8°$ (270 beamwidths scan at 230 GHz), the worst calculated beam efficiency is 95 percent. To cover such a wide frequency and scan range, each of the 28 plates is individually controlled for a tilting less than 4°, and for a sliding less than 0.5 cm. The sliding is done at discrete steps. At 230 GHz, a step size of 2 mil is sufficient. The plate positions must be reset for each frequency and for each scan direction. Once the position is set, the frequency bandwidth of the antenna is very narrow.

17. Key Words (Suggested by Author(s))	18. Distribution Statement
Radiometers Beam waveguides Physical optics Electromagnetic analysis	Unclassified – Unlimited Subject Category 32

19. Security Classif. (of this report)	20. Security Classif. (of this page)	21. No of pages	22. Price*
Unclassified	Unclassified	39	A03

NASA FORM 1626 OCT 86

*For sale by the National Technical Information Service, Springfield, Virginia 22161